journal homepage: www.intl.elsevierhealth.com/journals/cmpb

# Single subject image analysis using the complex general linear model—An application to functional magnetic resonance imaging with multiple inputs

*Daniel E. Rio*[a,*], *Robert R. Rawlings*[a], *Lawrence A. Woltz*[b], *Jasmin B. Salloum*[a], *Daniel W. Hommer*[a]

[a] *Section of Brain Electrophysiology and Imaging, Laboratory of Clinical Studies, National Institute on Alcohol Abuse and Alcoholism, National Institutes of Health, Bethesda, MD 20892, United States*

[b] *Synergy Research Inc., 12051 Greystone Dr., Monrovia, MD 21770, United States*

ARTICLE INFO

*Article history:*
Received 30 January 2005
Received in revised form 20 December 2005
Accepted 30 December 2005

*Keywords:*
Functional MRI
Image processing
Time series analysis
Fourier analysis
Statistics

ABSTRACT

A linear time invariant model is applied to functional fMRI blood flow data. Based on traditional time series analysis, this model assumes that the fMRI stochastic output sequence can be determined by a constant plus a linear filter (hemodynamic response function) of several fixed deterministic inputs and an error term assumed stationary with zero mean. The input function consists of multiple exponential distributed (time delay between images) visual stimuli consisting of negative and erotic images. No a priori assumptions are made about the hemodynamic response function that, in essence, is calculated at each spatial position from the data. The sampling rate for the experiment is 400 ms in order to allow for filtering out higher frequencies associated with the cardiac rate. Since the statistical analysis is carried out in the Fourier domain, temporal correlation problems associated with inference in the time domain are avoided. This formal model easily lends itself to further development based on previously developed statistical techniques.

Published by Elsevier Ireland Ltd.

## 1. Introduction

The use of functional magnetic resonance images (fMRI) to study local changes in cerebral blood oxygenation is an important field of study. These functional magnetic resonance imaging (fMRI) studies often take the form of an input–output system where the input stimulus is used to elicit a hemodynamic response in the brain. Hemodynamic responses can then be indirectly measured using multiple $T_2^*$-weighted echo-planer magnetic resonance scans. These scans produce data that consist of a set of three-dimensional voxels covering all or part of the brain, where each voxel is composed of a series of time points. It is this time series (along with that of the input stimulus) that is used to discern whether a response has occurred. Thus, the problem is to use these time series within the context of a mathematical model that allows us to estimate the statistical significance of the hemodynamic response of the brain to the input stimulus. There are numerous problems inherent in carrying out this calculation, as the fMRI signal also includes various sources of noise as well as the results of the intrinsic hemodynamic filtering that occurs in the brain. This leads to a response that is both temporally shifted and blurred because of the hemodynamic filter and has noise layered on top of it. This problem is further complicated by the inherent temporal correlation in the data that can compromise the assignment of statistical significance [1–3]. Attempts

* *Corresponding author at*: NIAAA, NIH, Bldg. 10, CRC, Rm 2-2332, 10 Center Dr., MSC 1540, Bethesda, MD 20892-1540, United States. E-mail address: drio@nih.gov (D.E. Rio).

0169-2607/$ – see front matter. Published by Elsevier Ireland Ltd.
doi:10.1016/j.cmpb.2005.12.003

at handling the temporal autocorrelation problem have been previously addressed by band-pass filtering, prewhitening or coloring and extensively studied [4,5].

While most analysis techniques have been used to process these data in the temporal domain [6], some of the more interesting studies have involved the use of the frequency domain to mitigate the effects of this temporal correlation [7,8]. These techniques have worked best with experimental designs using a boxcar or single event with fixed interstimulus interval [7,8]. While a periodic stimulus has an obvious advantage in frequency-based analyses, the methodology to be presented in this paper can deal with any general input stimulus that is periodic or non-periodic in structure.

Furthermore, none of the previous frequency based analysis methods have been based on a unified hypothesis-testing formulation of this problem even though this has been a well-studied area of mathematical statistics [9–11]. A model is presented to analyze what are essentially traditional time series data embedded in a three-dimensional spatial array. By direct generalization, this model can be extended to fMRI data where the parameters correspond to multidimensional Euclidean spatial coordinates. In particular this model is based on statistical analyses of the general linear model in the frequency domain [9,12–14]. From a statistical point of view, analysis in the spectral domain presents an obvious methodological advantage when there is correlation in the temporal domain because, asymptotically, correlation between statistics at different frequencies is absent in the spectral domain [9].

In this paper, a number of hypothesis-based statistical tests using this model are presented and applied to a fMRI dataset obtained using non-periodic pseudo-Poisson process input stimuli with a very fast sampling rate. A localized estimation is made of the hemodynamic transfer function and sample results for a number of subjects are displayed.

## 2. Linear time invariant model

### 2.1. Basics

Let $s(\underline{x}, t)$ be a univariate stochastic field with multivariate spatial index $\underline{x} = (x_1, x_2, x_3)$ and temporal variable $t$ that corresponds to a four-dimensional functional image. In this case $s(\underline{x}, t)$ represents an fMRI signal [10]. If the input sequence $r(t)$ is a $R \times 1$ vector consisting of $R$ deterministic inputs functions of time and $a(\underline{x}, t)$ is a $1 \times R$ filter with multivariate spatial index $\underline{x}$, then the stochastic output is given by

$$s(\underline{x}, t) = \mu(\underline{x}) + \sum_{u=-\infty}^{\infty} a(\underline{x}, t-u)r(u) + \varepsilon(\underline{x}, t) \tag{1}$$

where $\mu(\underline{x})$ is a constant and $\varepsilon(\underline{x}, t)$ is the error at each given point. At each spatial position $\varepsilon(\underline{x}, t)$ is assumed stationary with zero mean. Take the temporal variable $t$ to be size $T$ and let the multivariate spatial variable $\underline{x}$ define some region of interest within the image. Thus, $s(\underline{x}, t)$ and $\varepsilon(\underline{x}, t)$ consist of $1 \times T$ vectors of random variables at each spatial position $\underline{x}$. In particular $s(\underline{x}, t)$ is a sequence, length $T$ in time, of three-dimensional fMRI images, and $\varepsilon(\underline{x}, t)$ is the associated noise in these images. A diagram of the model is presented in Fig. 1 for a $2 \times 1$ input vector relevant to the application in this paper.

Using this as our model it is possible to construct statistical tests in the Fourier domain. The one-dimensional Fourier transforms of $r(t)$, $a(\underline{x}, t)$ and $s(\underline{x}, t)$ from (1) in the temporal domain are given by

$$\tilde{r}(k) = T^{-1/2}\sum_{t=0}^{T-1} r(t)e^{-i\lambda_k t}, \qquad \tilde{a}(\underline{x}, k) = T^{-1/2}\sum_{t=0}^{T-1} a(\underline{x}, t)e^{-i\lambda_k t} \tag{2}$$

and

$$\tilde{s}(\underline{x}, k) = T^{-1/2}\sum_{t=0}^{T-1} s(\underline{x}, t)e^{-i\lambda_k t}$$

respectively where $\lambda_k = 2\pi k/T$ and $k$ represents the $k$th wave number.

The following periodogram functions:

$$\begin{aligned}
I_{sr}(\underline{x}, \lambda_k) &= (2\pi T)^{-1}\tilde{s}(\underline{x}, \lambda_k)\overline{\tilde{r}(\lambda_k)}^T, \quad a\ 1 \times R\ \text{vector};\\
I_{rs}(\underline{x}, \lambda_k) &= (2\pi T)^{-1}\tilde{r}(\lambda_k)\overline{\tilde{s}(\underline{x}, \lambda_k)}^T, \quad a\ R \times 1\ \text{vector};\\
I_{rr}(\lambda_k) &= (2\pi T)^{-1}\tilde{r}(\lambda_k)\overline{\tilde{r}(\lambda_k)}^T, \quad a\ R \times R\ \text{matrix};\\
I_{ss}(\underline{x}, \lambda_k) &= (2\pi T)^{-1}\tilde{s}(\underline{x}, \lambda_k)\overline{\tilde{s}(\underline{x}, \lambda_k)}^T, \quad a\ 1 \times 1\ \text{scalar}
\end{aligned} \tag{3}$$

($R$ dimensions are a consequence of having $R$ input functions) are constructed from the Fourier transform of the input function and the output (fMRI signal) function (2).

Estimates of the cross-spectral functions can be constructed from these periodograms. Furthermore, by constructing these estimates over disjoint frequency bands size $k = -m$ to $m$ centered at $\lambda$, more stable estimates of the cross-spectral functions may be obtained. Thus, using (3) the multivariate cross spectral functions are constructed as follows:

$$\begin{aligned}
f_{sr}(\underline{x}, \lambda) &= (2m+1)^{-1}\sum_{k=-m}^{m} I_{sr}(\underline{x}, \lambda + \lambda_k),\\
f_{rs}(\underline{x}, \lambda) &= (2m+1)^{-1}\sum_{k=-m}^{m} I_{rs}(\underline{x}, \lambda + \lambda_k),\\
f_{rr}(\lambda) &= (2m+1)^{-1}\sum_{k=-m}^{m} I_{rr}(\lambda + \lambda_k),\\
f_{ss}(\underline{x}, \lambda) &= (2m+1)^{-1}\sum_{k=-m}^{m} I_{ss}(\underline{x}, \lambda + \lambda_k)
\end{aligned} \tag{4}$$

where $\lambda$ is the center frequency of each disjoint band. These take a slightly different form for even or odd spectral ranges and at the end points of the spectrum [9,15]. The functions $f_{rr}(\lambda)$ and $f_{ss}(\underline{x}, \lambda)$ are the power spectra of the input and output (fMRI) of the system, respectively.

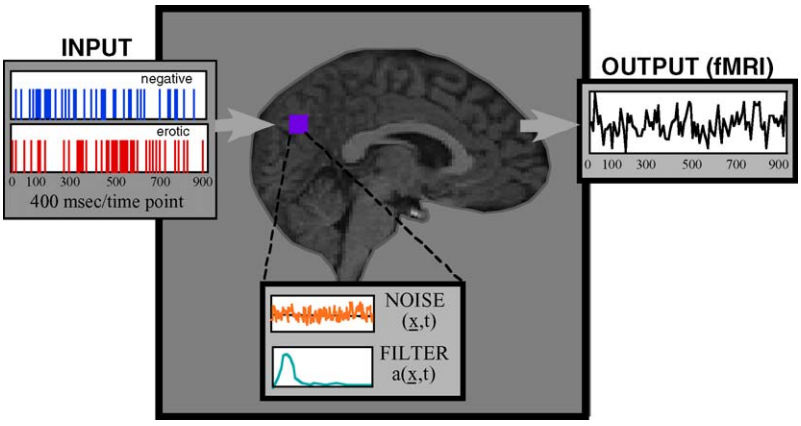


**Fig. 1 – Diagrammatic representation of the mathematical model used to statistically analyze data where multiple inputs are presented to the subject. The subject processes these input stimuli and an output indicator is measured (the fMRI signal). This output signal is seen to be affected by a filter (the hemodynamic transfer function in this case) and various sources of noise (both biological and acquisition based).**

### 2.2. *Hypothesis testing*

If at each spatial position $\underline{x}$, the expectation value $E[\tilde{\varepsilon}(\underline{x}, \lambda)] = 0$ and

$$E[\tilde{\varepsilon}(\underline{x}, \lambda)\,\overline{\tilde{\varepsilon}(\underline{x}, \lambda)}] = 2\pi T f_{\varepsilon\varepsilon}(\underline{x}, \lambda) \tag{5}$$

where $f_{\varepsilon\varepsilon}(\underline{x}, \lambda)$ is called the error spectrum, then by application of the complex form of the Gauss–Markov theorem and taking into account the distributional attributes of the variables, $F$-tests may be set up [12,16]. Consider the test of the hypothesis $H_0: \tilde{a}(\underline{x}, \lambda) = 0$ at each spatial position and wave number. This takes the form of the following $F$-test:

$$F(\underline{x}, \lambda)_{2R;2(2m+1-R)} = \frac{(2m+1)\hat{A}(\underline{x}, \lambda) f_{rr}(\lambda)\overline{\hat{A}(\underline{x}, \lambda)^T}}{R g_{\varepsilon\varepsilon}(\underline{x}, \lambda)} \tag{6}$$

where

$$\hat{A}(\underline{x}, \lambda) = f_{sr}(\underline{x}, \lambda)[f_{rr}(\lambda)]^{-1} \tag{7}$$

is an estimate of the transfer function $\tilde{a}(\underline{x}, \lambda)$ (filter in the frequency domain). Furthermore, using (4), an estimate of the error spectrum can be constructed as:

$$g_{\varepsilon\varepsilon}(\underline{x}, \lambda) = \frac{2m+1}{2m+1-R}\left\{f_{ss}(\underline{x}, \lambda) - f_{sr}(\underline{x}, \lambda)[f_{rr}(\lambda)]^{-1} f_{rs}(\underline{x}, \lambda)\right\} \tag{8}$$

This estimate of the error spectrum $f_{\varepsilon\varepsilon}(\underline{x}, \lambda)$ indicates how well the linear time invariant model fits the data.

Further tests similar to the general $F$-test for activation can be constructed to compare and contrast the multiple inputs, $r(t)$ [12]. The hypotheses to be tested now take the form $H_0: \tilde{a}(\underline{x}, \lambda)B = 0$ where the $F$-test is constructed as follows:

$$F(\underline{x}, \lambda)_{2(R-1);2(2m+1-R)} = \frac{(2m+1)\hat{A}(\underline{x}, \lambda)B[B^T[f_{rr}(\lambda)]^{-1}B]^{-1}B^T\overline{\hat{A}(\underline{x}, \lambda)^T}}{(R-1)g_{\varepsilon\varepsilon}(\underline{x}, \lambda)} \tag{9}$$

where $B$ is an $R \times (R-1)$ matrix used to test various components of the input vector $r(t)$.

All other terms have been previously defined in Eqs. (4) and (7). Note again that $R$ is the number of input time functions and $2m+1$ is the size of the disjoint bands. Using these constructed values it is possible to test for activation caused by the response of the system to each component of the input function at each spatial position of interest and wave number $\lambda$ and, furthermore also test whether there is a differential response between the various components. Generally care must be taken when applying this test for bands with low input power as this test becomes invalid because of numerical instability.

## 3. Application

### 3.1. *Experimental design*

As a demonstration of the methodology, a set of five male subjects aged 21–35 years, was investigated from a larger set of data using event related fMRI. The general focus of this study was to study the neural substrates of arousal using a combination of erotic and negative stimuli. Additional considerations in designing this study were to achieve high rate sampling within the context of a short duration experiment. Hence a high sampling rate of $T_R = 400$ ms was chosen along with stimulus presentation time of 800 ms. Studies have shown that a change in feelings can be evoked in subjects with stimulus presentations of 500 ms outside of the scanner [17]. The combination of high sampling rate and analysis in the frequency domain enables the application of filters to eliminate some cardiac and motion artifacts. For high sampling rates and large $T$ during multislice imaging, it has been shown that it is possible to distinguish frequencies of respiratory and cardiac noise [18]. Finally, it was also likely that a short duration experiment would reduce patient movement and also allow the subjects to remain focused on the task at hand.

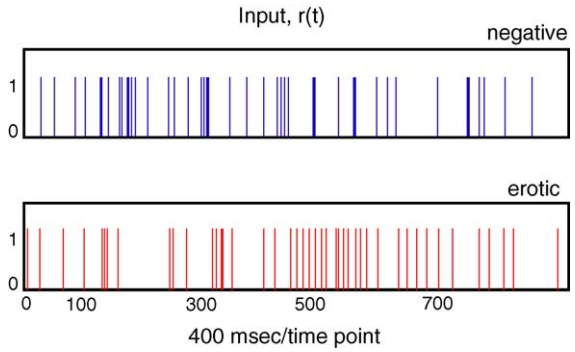


**Fig. 2 – Diagram showing the Poisson input stimulus timing where each time point is 400 ms long. Each vertical blue line represents an 800 ms presentation of a negative image to the subject and each vertical red line an erotic image also presented for 800 ms. For interpretation of the references to colour in this figure legend, the reader is referred to the web version of the article.**

### 3.2. *Pseudo-Poisson input*

In Fig. 2 each line represents a visual presentation of either negative (blue) or erotic (red) images each having a duration of 800 ms. The time interval between each image has been derived from an exponential distribution. These distributions were generated until little or no overlap occurred between the two selected input functions. In a few instances where overlap occurred, the image presentations were randomly shifted 400 ms up or down until no overlap occurred.

For an ideal Poisson process these input functions would distribute power equally at all frequencies in the power spectrum. Of course in this case, where the stimulus is finite and the sampling is discrete (in this case a sampling rate of 400 ms), the shape of the power spectra is compromised from this ideal case as can be seen in Fig. 3. Thus, the power spectrum is not uniform from frequency to frequency and decreases in power at higher frequencies. This feature would subside for longer duration experiments and the high frequency fall off would decrease for increasing short sampling rates with point stimulations.

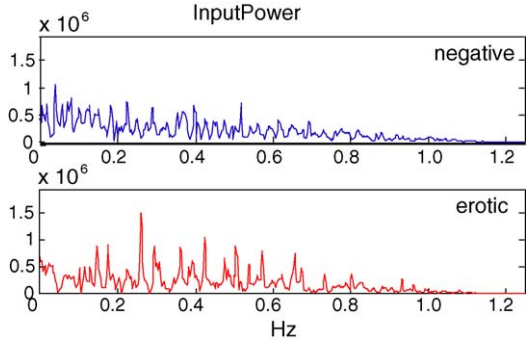


**Fig. 3 – A plot of the Poisson power distribution for the negative (blue) and erotic (red) inputs. For interpretation of the references to colour in this figure legend, the reader is referred to the web version of the article.**

### 3.3. *Image acquisition and preprocessing*

The subjects were exposed to erotic and negative slides (pseudo-Poisson process) using the Affective Picture System [19] matched for arousal (erotic = 5.95 with S.D. = 0.93; negative = 5.94 with S.D. = 1.25) and scrambled control images during two runs each lasting 6.4 min. An arousal level of 5.95 on this scale is considered very high. The images were projected onto a screen in the scanner room. Ten contiguous oblique-axial slices were acquired of the limbic area (5 slices) and frontal/orbitofrontal areas (5 slices). During the task, 910 $T_2^*$-weighted echo-planer MR volumes ($T_R$ = 400 ms, $T_E$ = 19.2 ms, flip angle = 60°, FOV = 24 cm, slice thickness = 5 mm, gap = 1 mm) were collected using a 1.5 T magnet (Medical Advances, Milwaukee, WI), resulting in a voxel size of 3.75 mm × 3.75 mm × 5 mm. The first 10 slices were collected before the visual presentations of negative and erotic images began. Sequences of runs as well as stimulus presentations were counterbalanced. One hundred and twenty-four $T_1$-weighted coronal SPGR images ($T_R$ 27 = ms, $T_E$ = 3.0 ms, flip angle = 45°, BW = 15.63, FOV = 24, slice thickness = 2 mm) were also acquired, resulting in a voxel size of 0.9375 mm × 0.9375 mm × 2 mm.

The first 10 time points, collected before the image presentations began, were discarded. The motion correction algorithm implemented in the AFNI [20] was applied to the functional data. Co-registration of the function scans to the anatomical scan was also performed in AFNI using landmark identification.

### 3.4. *Computational information*

For preprocessing, the AFNI software package used was installed on an AMD clone PC (equivalent to a 2.5 GHz Intel Pentium processor PC) with 2 GB of memory running RedHat Linux 9.0. The bulk of the calculations used the image processing software package SRView running on an Apple 1.8 GHz G5 computer with 1.5 GB of memory. This image processing software was developed by Synergy Research Inc., 12051 Greystone Dr., Monrovia, MD, 21770 in conjunction with the staff from the National Institute on Alcohol Abuse and Alcoholism. The mathematical, statistical and image presentation programs were written in C, C++ and Motif. Tcl/Tk is used as the scripting language to integrate more complex calculations or make bulk runs. A typical analysis took less than 30 min of computational time per subject when all steps from initial alignment to completed statistical analysis were included. In particular the statistical analysis discussed in this paper required only about 5 min of computational time on the Apple computer. This software also has been implemented on other computers running Unix and Linux operating systems.

### 3.5. *Image processing*

Once the functional images were aligned, the first four time points were removed from them along with the first four points of the input functions to remove scanner transients. Then a two-dimensional spatial Gaussian filter, full width half maximum (FWHM) equal to 4 mm, was applied. Lastly a low

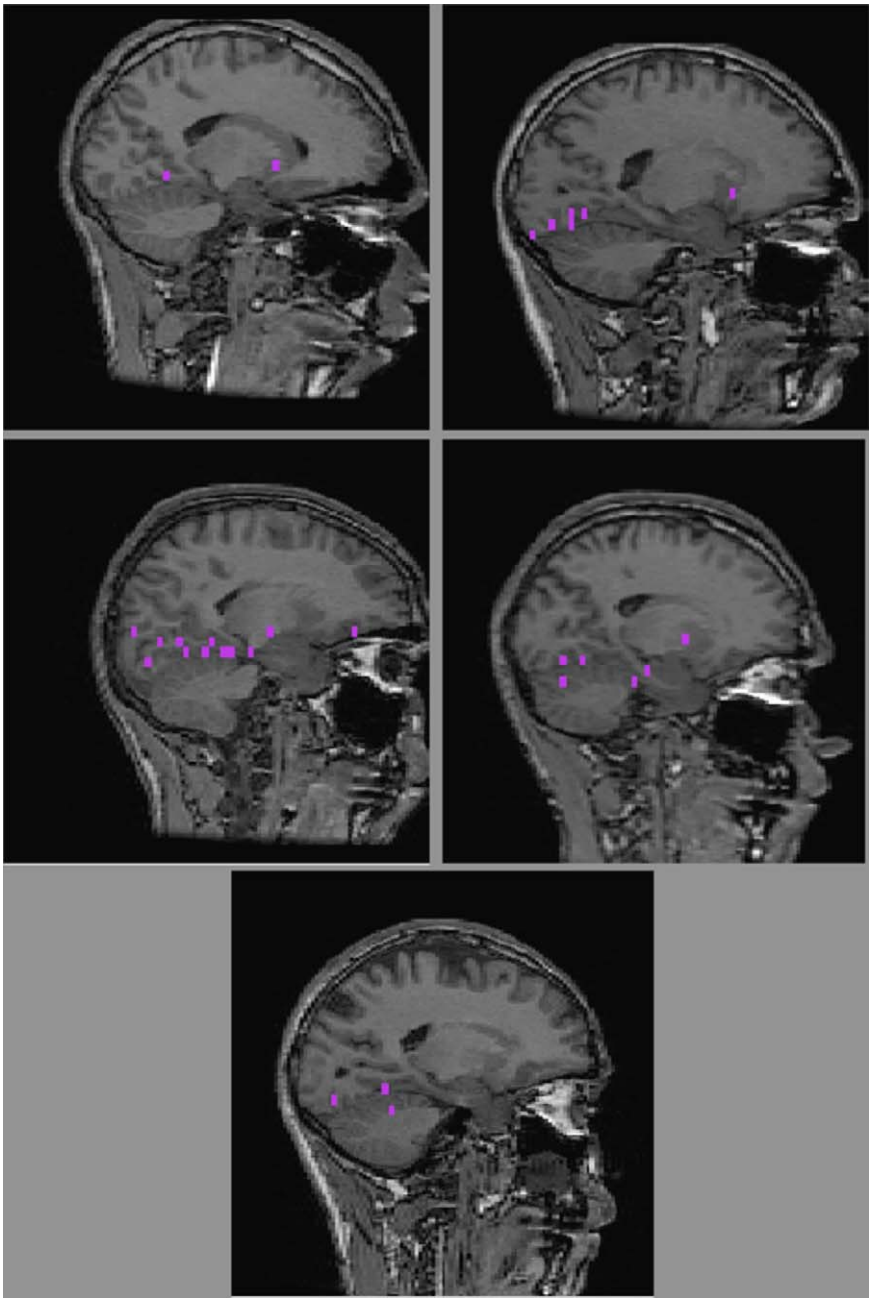

**Fig. 4 – The general F-test (case 1-purple mask) shows activated voxels in the lingual and parahippocampal gyri of all five subjects. For interpretation of the references to colour in this figure legend, the reader is referred to the web version of the article.**

pass filter was applied and all frequencies above 0.9 Hz were removed from the fMRI signals to suppress some cardiac and respiratory artifacts.

## 4. Results

### 4.1. *Hypothesis testing*

A number of significance tests can be performed with various null hypotheses. These test whether the input stimuli (that is, negative and erotic sequence of images) together or individually elicit a response in the fMRI output series. Furthermore, it is also possible to test those voxels for a differential response to the negative and erotic input stimuli.

For the input consisting of the two generated sequences of images, $R$ is set to 2 in (3) and the remaining Eqs. ((4)–(7)). Eq. (5) is then used to test for a general response to the input. Thus, the omnibus test for the general response to the input is

Case 1 : test the hypothesis $H_0 : \tilde{a}(\underline{x}, \lambda) = 0$

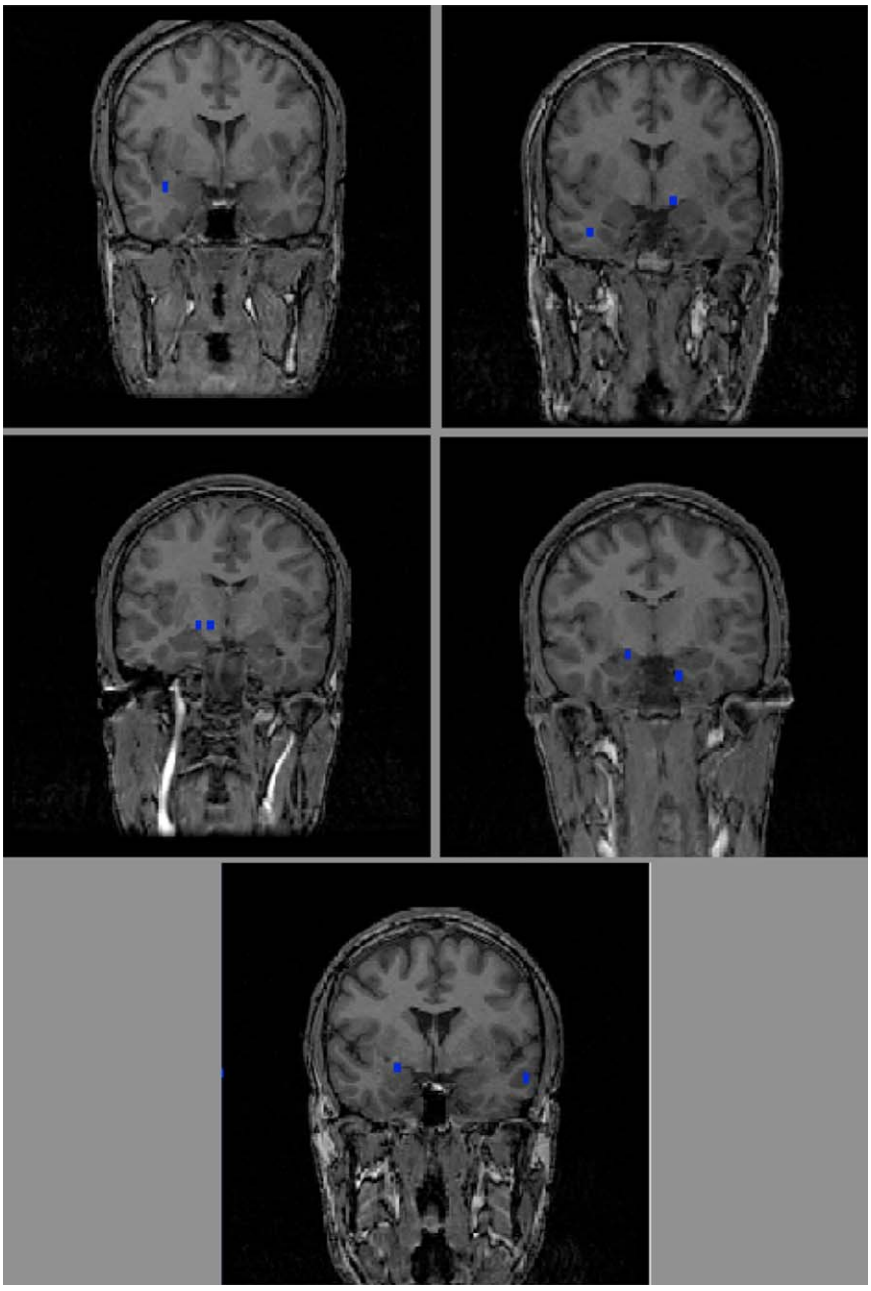

**Fig. 5 – Voxels activated by the negative images (case 2-blue mask) are found in the amygdala and sub-lenticular extended amygdala in four of the five subjects. For interpretation of the references to colour in this figure legend, the reader is referred to the web version of the article.**

The size of the bands (number of support frequencies) was set to 13 or $m = 6$ in Eqs. (3)–(9) giving 33 bands to test. The first band is centered at wave number 0 and the remaining disjoint bands fill the frequencies up to the Nyquist frequency (note that since a low pass filter was used on the fMRI data, tests were restricted to frequencies below 0.9 Hz). Thus, sets of $F$-test images based on Eq. (6) were constructed. The significance level was set to $\alpha = 0.0005$ divided by 33 and tests were made at each voxel and band. The expected false positive rate was approximately three for the number of tests performed.

The following $F$-tests were also performed for those voxels that tested positive for case 1. Using Eq. (9) it is possible to choose $B$ as follows to perform hypothesis testing on the specific negative and erotic input:

$$\text{Case 2}: \quad B = \begin{pmatrix} 1 \\ 0 \end{pmatrix},$$

test the hypothesis $H_0: \ \tilde{a}(\underset{\sim}{x}, \lambda)B = 0$

for response to the negative image input

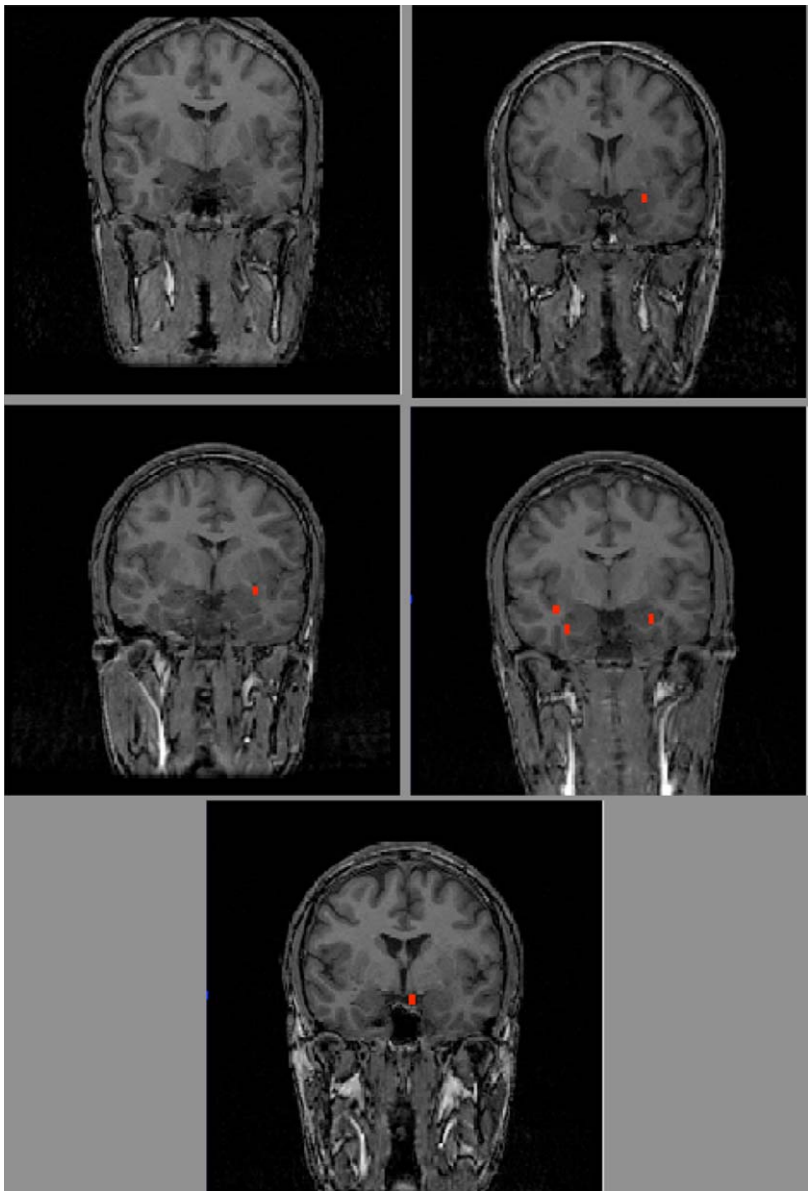

**Fig. 6 – Presentation of the erotic images activated voxels (case 3-red mask) in the amygdala and sub-lenticular extended amygdala in four of the five subjects. However, while these activated voxels appeared in the same anatomical regions they did not correspond to those voxels activated by the negative images (see Fig. 5). The subjects without amygdala activation show activation in the right hippocampus. For interpretation of the references to colour in this figure legend, the reader is referred to the web version of the article.**

Case 3 : $B = \begin{pmatrix} 0 \\ 1 \end{pmatrix}$,

test the hypothesis $H_0$ : $\tilde{a}(\underline{x}, \lambda)B = 0$

for response to the erotic image input

Case 4 : $B = \begin{pmatrix} -1 \\ 1 \end{pmatrix}$,

test the hypothesis $H_0$ : $\tilde{a}(\underline{x}, \lambda)B = 0$

for differential response to the negative and erotic image inputs

These tests are performed for each frequency band and, while it may be of some interest to note the frequencies that give a significant response for the applied input, in this paper a cumulative mask was constructed to present most of the results as follows. A binary mask was produced for each band, where a value of 1 was assigned for a positive response (i.e., when the hypothesis was non-zero). Then the masks from each band were ORed together, except for the 0 band. Thus, the resultant masks represent a response at any frequency band that occurred to the input at that spatial position. The band centered at 0 was omitted to limit low frequency drift, some of which may be caused by subject movement.

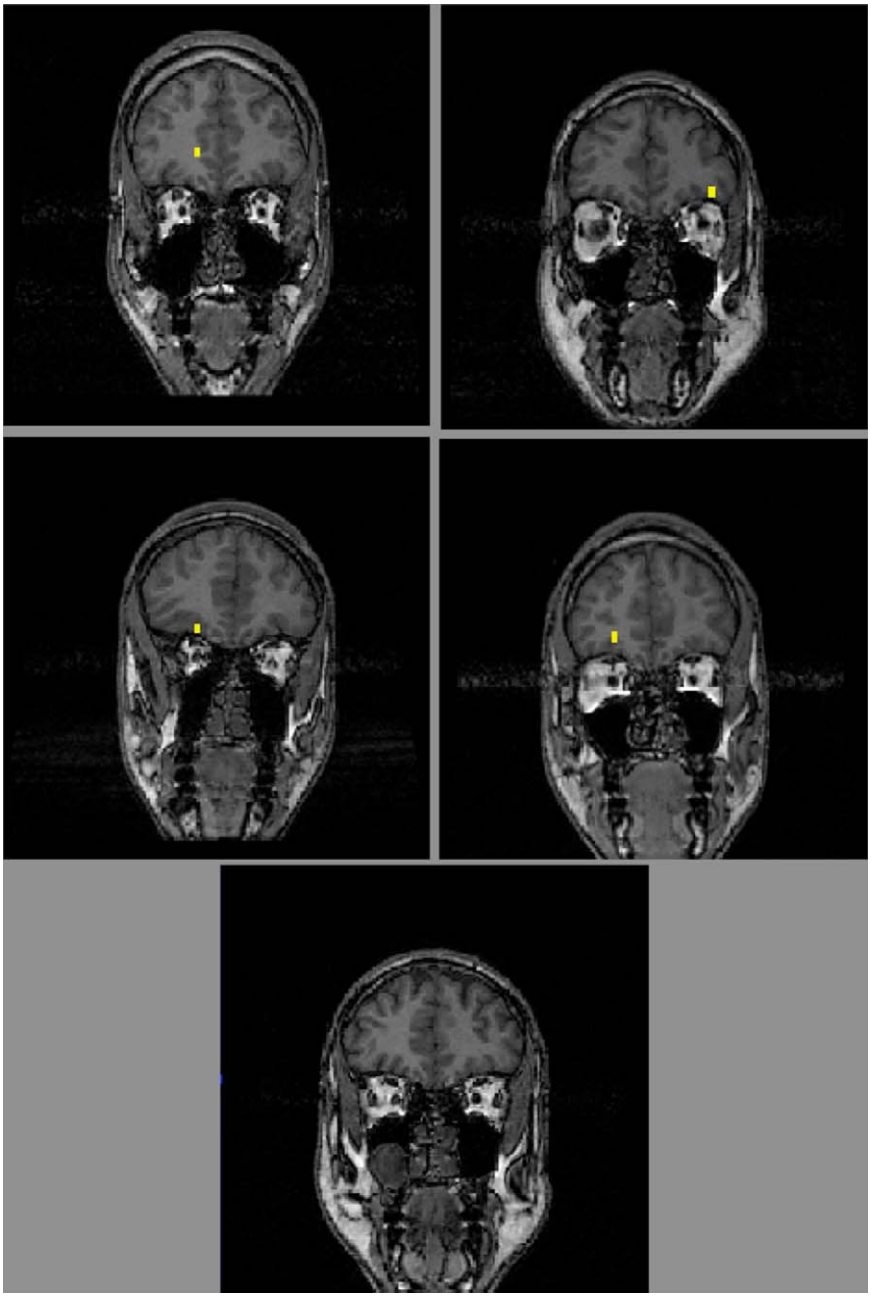

**Fig. 7 – Voxels in the right lateral orbital gyrus showed differential activation (case 4-yellow mask) between negative and erotic images in four of the five subjects. For interpretation of the references to colour in this figure legend, the reader is referred to the web version of the article.**

Several brain regions were used as representative regions to show results from the four *F*-test cases. These regions were the lingual and parahippocampal gyri, the amygdala and sublenticular extended amygdala and the orbital cortex.

The results of the general *F*-test for the five subjects are presented in Fig. 4 (case 1-purple mask). Fig. 5 depicts the response to the negative image presentation (case 2-blue mask) and Fig. 6 to the erotic image input (case 3-red mask). Finally, Fig. 7 (case 4-yellow mask) presents those voxels in which the negative and erotic response was different. Note again that only those voxels that responded to the general input case 1 were tested for cases 2–4.

### 4.2. *A closer look at the analysis in the frequency domain*

Using (4), $f_{rr}(\lambda)$, the banded spectral power of the input stimuli is obtained. This is presented in Fig. 8 and includes both the lowest frequency band as well as the higher frequency bands before a low pass filter was applied (bands not used in the hypothesis testing). Some similarity with the power spectra obtained at each frequency in Fig. 3 can be discerned.

To demonstrate a response of the output signal, $s(\underline{x}, t)$ to the input, a number of graphs are presented for both an inac-

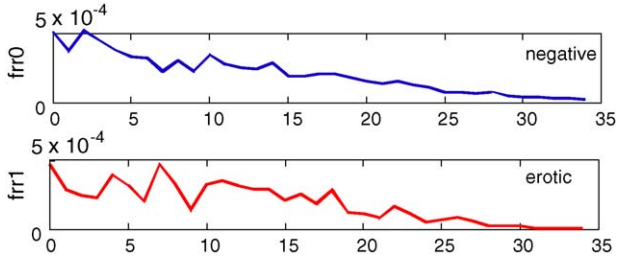


**Fig. 8 – A plot of the cross-spectral functions $f_{rr}(\lambda)$ for the 33 bands used in the analysis. Similar to the power spectra plotted in Fig. 3, each band is 0.0335 Hz wide (for example the band labeled 1 includes frequencies from 0.0195 to 0.0530 Hz) including the zero-centered frequency band that is calculated using the symmetry in the Fourier spectrum.**

tivated voxel (Fig. 9) and activated voxel (Fig. 10). Firstly, the banded spectral density function, $f_{ss}(\underline{x}, \lambda)$ of the output or fMRI signal, $s(\underline{x}, t)$ is graphed. Beneath this graph the banded *F*-test (6) results for case 1, testing the hypothesis $H_0: a(\underline{x}, \lambda) = 0$, is plotted, along with the threshold value for the *F*-statistic equal to 7.67 (the dashed line), calculated for $\alpha = 0.0005$ divided by 33 bands as noted previously. Values for the *F*-statistic above threshold show the statistically significant frequency bands. For the inactivated voxel there are none while for the activated voxel two bands centered at 0.0530 Hz (band 1) and 0.1256 Hz (band 3) show a response to the input stimulus. Finally, the bottom graph in Figs. 9 and 10 show the error spectra $g_{\varepsilon\varepsilon}(\underline{x}, \lambda)$, that is seen to be much smaller for the activated voxel.

Comparing these graphs for the activated voxel (Fig. 10) to the graphs for the inactivated voxel (Fig. 9) clearly shows the differences between the voxels, with the activated voxel having *F* values that are significant and an error spectrum that is much smaller than that for the inactivated voxel. While a lower error spectrum is not a necessary condition for activation, it usually is low in voxels in which activation can be seen.

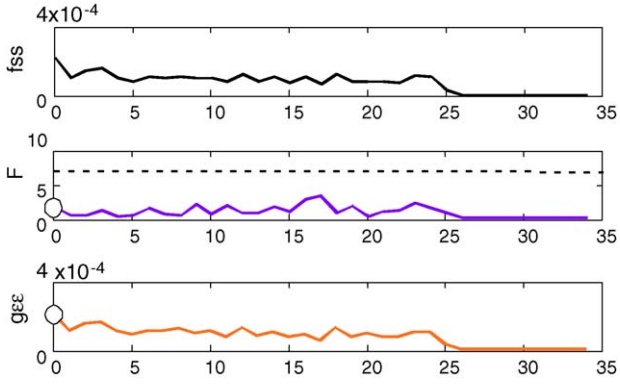


**Fig. 9 – Plots of the cross-spectral functions $f_{ss}(\underline{x}, \lambda)$-(top plot-based on Eq. (4)), *F*-test spectral function for the general test $F(\underline{x}, \lambda)$ (center plot-purple line, based on Eq. (6)); and error function, $g_{\varepsilon\varepsilon}(\underline{x}, \lambda)$ (bottom-orange line, based on Eq. (9)) for the 33 bands used in the analysis for a particular non-activated voxel. The center plot for the *F*-test function also shows the threshold for activation as a dashed line. For interpretation of the references to colour in this figure legend, the reader is referred to the web version of the article.**

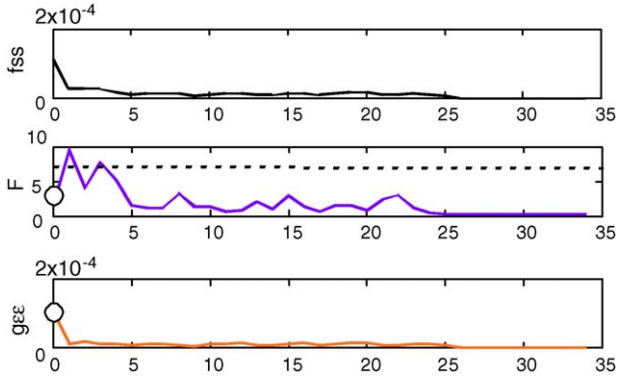


**Fig. 10 – Plots of the cross-spectral functions $f_{ss}(\underline{x}, \lambda)$-(top plot-based on Eq. (4)), *F*-test spectral function for the general test, $F(\underline{x}, \lambda)$ (center plot-purple line, based on Eq. (6)) and error function, $g_{\varepsilon\varepsilon}(\underline{x}, \lambda)$ (bottom-orange line, based on Eq. (9)) for the 33 bands used in the analysis for a particular activated voxel. The center plot for the *F*-test function also shows the threshold for activation as a dashed line. For interpretation of the references to colour in this figure legend, the reader is referred to the web version of the article.**

## 5. Conclusion

We present a general linear model in the Fourier domain for which numerous *F*-tests can be constructed to test multiple input evoked responses. Problems with temporal correlation are avoided by performing the statistics in the Fourier domain. Also no a priori assumptions need be made about the filter in applying this model, and estimates of the corresponding hemodynamic transfer function are obtained at each spatial location for the volumetric image. Additional features of this methodology will also allow testing for differences in the hemodynamic transfer function at different spatial locations or different experimental conditions.

To demonstration the usefulness of this methodology for non-periodic and short interstimulus intervals, multiple input stimuli of duration 800 ms were used in an fMRI experiment with a $T_R$ of 400 ms. This allows for a short duration experiment that reduces subject movement confounds, and allows for filtering of unwanted physiological processes that may interfere with the evoked response.

Furthermore, since this methodology shows particular promise for single subject analysis studies are currently being designed to apply it in a clinical setting. Toward this end experimental protocols using fearful images (to be presented in a similar fashion to that for the input images in this study) will be used to study a group of subjects who perpetrate acts of domestic violence [21,22].

## REFERENCES


[1] K. Friston, O. Josephs, E. Zarahn, A. Holmes, J.B. Poline, To smooth or not to smooth? Neuroimage 12 (2000) 196–208.

[2] P.L. Purdon, R.M. Weisskoff, Effect of temporal autocorrelation due to physiological noise and stimulus paradigm on voxel-level false-positive rates in fMRI, Hum Brain. Mapp. 6 (1998) 239–249.

[3] E. Zarahn, G. Aquirre, M. D'Esposito, Empirical analyses of BOLD fMRI statistics 1. Spatially unsmoothed data collected under null-hypothesis conditions, Neuroimage 5 (1997) 179–197.

[4] E. Bullmore, M. Brammer, S.C.R. Williams, S. Rabe-Hesketh, N. Janot, A. David, J. Mellers, R. Howard, P. Sham, Statistical methods of estimation and inference for functional MR image analysis, Magn. Reson. Med. 35 (1996) 261–277.

[5] M.W. Woolrich, B.D. Ripley, M. Brady, S.M. Smith, Temporal autocorrelation in univariate linear modeling of FMRI data, Neuroimage 14 (2001) 1370–1386.

[6] K. Worsley, K. Friston, Analysis of fMRI time series revisted—again, Neuroimage 2 (1995) 173–181.

[7] P. Bandettini, W. Cox, Event-related fMRI contrast when using constant interstimulus interval: theory and experiment, Magn. Reson. Med. 43 (2000) 450–548.

[8] J.L. Marchini, B.D. Ripley, A new statistical approach to detecting significant activation in functional MRI, Neuroimage 12 (2000) 366–380.

[9] D. Brillinger, TIME SERIES Data Analysis and Theory, Holden-Day, San Francisco, 1981.

[10] G.M. Jenkins, D.G. Watts, Spectral Analysis and its Applications, Holden-Day, San Francisco, 1969.

[11] L. Koopmans, The Spectral Analysis of Time Series, Academic Press, New York, 1974.

[12] D.R. Brillinger, The general linear model in the design and analysis of evoked response experiments, J. Theor. Neurobiol. 1 (1981) 105–119.

[13] D.R. Brillinger, Some statistical methods for random process data from seismology and neurophysiology, Ann. Statist. 16 (1988) 1–54.

[14] D.E. Rio, R.R. Rawlings, D.W. Hommer, Application of a linear time invariant model in the Fourier domain to perform statistical analysis of functional magnetic resonance images, in: C. Chen, A.V. Clough (Eds.), Physiology and Function from Multidimensional Images I, SPIE, Washington, 2000, pp. 265–275.

[15] D.R. Brillinger, The finite Fourier transform of a stationary process, in: D.R. Brillinger, P.R. Krishnaiah (Eds.), Time Series in the Frequency Domain. Handbook of Statistics, 3, North-Holland Publishing Co, Amsterdam, 1983, pp. 21–37.

[16] C.G. Khatri, Classical statistical analysis based on a certain multivariate complex Gaussian distribution, Ann. Math. Statist. 36 (1965) 98–114.

[17] G. McCarthy, A. Puce, M. Luby, A. Belger, T. Allison, Magnetic resonance imaging studies of functional brain activation: analysis and interpretation, in: Y.C. Okada, S. Ogawa (Eds.), Visualization of Information in the Human Brain: Recent Advances in MEG and Functional MRI, EEG Suppl. 47, Elsevier Science, 1996, pp. 15–31.

[18] D. Cordes, V.M. Haughton, K. Arfanakis, J.D. Carew, P.A. Turski, C.H. Mortiz, M.A. Quigley, M.E. Meyerand, Frequencies contributing to functional connectivity in the cerebral cortex in "resting-state" data, Am. J. Neuroradiol. 22 (2001) 1326–1333.

[19] P.J. Lang, M.M. Bradley, B.N. Cuthbert, International Affective Picture System (IAPS): Technical Manual and Affective Ratings, University of Florida, Gainesville, FL, 1997.

[20] R.W. Cox, AFNI: software for analysis and visualization of functional magnetic resonance neuroimages, Comp. Biomed. Res. 29 (1996) 162–173.

[21] D.T. George, J.R. Hibbeln, P.W. Ragan, J.C. Umhau, M.J. Phillips, L. Doty, D. Hommer, R.R. Rawlings, Lactate-induced rage and panic in a select group of subjects who perpetrate acts of domestic violence, Biol. Psychiatry 47 (2000) 804–812.

[22] D.T. George, R.R. Rawlings, W.A. Williams, M.J. Phillips, G. Fong, M. Kerich, R. Momenan, J.C. Umhau, D. Hommer, A select group of perpetrators of domestic violence: evidence of decreased metabolism in the right hypothalamus and reduced relationships between cortical/subcortical brain structures in positron emission tomography, Psychiatry Res. 130 (2004) 11–25.